ANALYSIS OF VIRAL SURFING BASED ON FLUORESCENCE MICROSCOPY IMAGING AND AUTOMATIC TRACKING

Vasil Tsimashchuk[1], *William J. Godinez*[1], *Maik Lehmann*[2], *and Karl Rohr*[1]

[1] University of Heidelberg, BioQuant, IPMB, and DKFZ Heidelberg,
Dept. Bioinformatics and Functional Genomics, Biomedical Computer Vision Group,
Im Neuenheimer Feld 267, 69120 Heidelberg, Germany
[2] Humboldt-University Berlin, Molecular Parasitology,
Philippstrasse 13, 10115 Berlin, Germany

ABSTRACT

Ordered movement of virus particles along cell filopodia before cell entry known as viral surfing is an important pathway for cell infection. To quantitatively analyze the process of viral surfing, tracking of viruses over time in fluorescent time-lapse microscopy images is required. We have developed an automatic approach for tracking single surfing virus particles. The approach combines probabilistic tracking of virus particles with a novel approach for segmentation of cell filopodia which is used to discriminate surfing virus particles. The approach was successfully applied to synthetic images as well as live cell microscopy images.

Index Terms— Microscopy image sequences, tracking virus particles, segmentation of cell filopodia

1. INTRODUCTION

Attachment of viruses to receptors on cell surface actin protrusions (filopodia) is followed by ordered lateral viral movement toward the cell body before cell entry [1]. This process is called "viral surfing" and viruses utilize cellular mechanisms for absorption of proteins and lipids [1, 2]. To study the influence of viral surfing on the infection rate and to identify cellular factors that regulate cell infection, it is important to analyze the dynamic behavior of surfing virus particles based on live cell microscopy images.

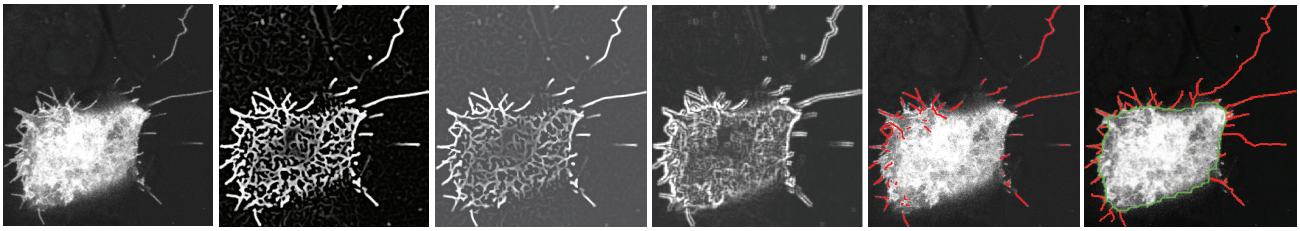
In previous work on analyzing viral surfing, only semi-automatic approaches have been used [1, 2]. There, the detection of virus particles was performed manually and tracking was carried out either manually or semi-automatically with manual correction of the trajectories. A completely automatic approach has not yet been proposed for the analysis of viral surfing. For the general problem of tracking virus particles (e.g., [3, 4, 5, 6]) or other biological particles (e.g., [7]) automatic approaches have been used. Probabilistic methods based on Bayesian filtering (e.g., [4, 7, 5]) have been shown to yield improved results compared to deterministic methods (e.g., [3]). For multiple virus tracking, approaches based on particle filters [8] have been used successfully (e.g., [5]). In these approaches, the dynamical and measurement models can be represented by non-linear non-Gaussian models.

A drawback of previous automatic tracking approaches for virus particles is that all particles within an image are tracked irrespective of a specific biological context. Thus, these approaches do not distinguish, for example, whether the particles move outside a cell or enter a cell. Quantitative analysis of viral surfing requires tracking of only those virus particles that move along cell filopodia. Therefore, virus particles should be tracked only when they attach to cell filopodia and tracking should be finished as soon as they invade cells. However, previous automatic tracking approaches track all virus particles and thus cannot be directly applied to the problem of analyzing viral surfing.

Here, we propose a novel approach for automatic analysis and quantification of the movement of virus particles during viral surfing. The approach combines a probabilistic approach for tracking virus particles with a novel approach for segmentation of cell filopodia. Thus, only those virus particles are tracked which move along cell filopodia. We also introduce a technique to determine the motion direction and speed of surfing virus particles relative to the cell body. We have successfully applied our approach to synthetic images as well as to real microscopy image sequences displaying virus-cell interactions.

2. METHODS

In the first step of our approach, cell filopodia are segmented and virus particles are detected. Second, the segmentation result is used to discriminate surfing virus particles from other particles. Third, a probabilistic tracking approach based on independent particle filters is used for tracking surfing virus particles. Fourth, the direction and speed of the movement of surfing virus particles towards or away from a cell are determined.



(a) Original image (b) Vesselness filter (c) Matched filter (d) GD filter (e) GD-based NMS (f) Final result

Fig. 1. Segmentation of cell filopodia (red). The outline of the cell body is shown by a green contour.



(a) (b)

Fig. 2. Cross-sections of responses of the GD filter to (a) a line structure and (b) a step edge structure.

2.1. Segmentation of Cell Filopodia

To discriminate surfing virus particles from other virus particles, we segment cell filopodia at each time point of an image sequence. Filopodia are represented as thin elongated structures originating at the borders of cell bodies. Segmentation of filopodia is difficult because these structures are very thin and they strongly change their shape over time. To segment filopodia, we first perform thin structure enhancement. We have used two different approaches for enhancing thin structures.

The first approach for enhancing filopodia structures uses a vesselness filter [9] (see the result in Fig. 1(b) for the original image in (a)). The second approach is based on a matched filter [10] with the kernel

$$K_{MF}(x,y,\alpha) = \frac{1}{\sqrt{2\pi}\sigma} e^{-\frac{(x\cos\alpha - y\sin\alpha)^2}{2\sigma^2}} - m, \quad (1)$$

where $\alpha \in [0,\pi)$ is the filter orientation, σ represents the scale of the filter, and m is a normalization constant (see the result in Fig. 1(c)). However, a disadvantage of directly applying these approaches is that they produce a high response both at filopodia (thin line structures) and at cell borders (step edge structures), which leads to false positive detections of filopodia.

To discriminate thin line structures (filopodia) from step edge structures (cell borders), we propose an approach based on the response of a Gaussian derivative (GD) filter, where the filter kernel is defined as

$$K_{GD}(x,y,\alpha) = -\frac{x\cos\alpha - y\sin\alpha}{\sqrt{2\pi}\sigma^3} e^{-\frac{(x\cos\alpha - y\sin\alpha)^2}{2\sigma^2}} \quad (2)$$

At each image point, the GD filter is applied in different directions $\alpha \in [0,\pi)$ and the maximum response of the filter is determined (Fig. 1(d)). Figure 2 shows cross-sections of the GD filter responses applied to an ideal line (i.e., a straight line with a Gaussian cross-section) and a step edge. For the ideal line a local minimum at the center is obtained. For a step edge, a local maximum at the center is obtained. We utilize this fact to detect thin line structures. We perform non-maximum suppression (NMS) and require that relevant line points are not only local maxima of the response of the thin structure enhancement in the direction of the image gradient but also local minima of the GD filter response (Fig. 1(e)).

However, using thin structure enhancement and NMS as described above often leads to segmented structures corresponding to the same filopodium, which are not connected (Fig. 1(e)). To improve the result, we use an approach based on the fast marching algorithm [11]. We compute the minimal action map $\mathcal{U}(\boldsymbol{z})$ as follows:

$$\mathcal{U}(\boldsymbol{z}) = \min_{\gamma \in \mathcal{A}_{\Omega,\boldsymbol{z}}} \left\{ \int_\gamma \tilde{\mathcal{P}}(\gamma(s))ds \right\} \quad (3)$$

where Ω is the region corresponding to the cell body and $\mathcal{A}_{\Omega,\boldsymbol{z}}$ is the set of all paths connecting a point $\boldsymbol{z}$ to Ω. As potential function we use $\tilde{\mathcal{P}} = \frac{1}{V} + w$, where V is the response of the thin structure enhancement, and w is a normalization constant. By using this approach, the segmented line fragments are now connected either with each other or with the cell body (Fig. 1(f)). To segment cell bodies, we first apply a median filter and a Gaussian filter to the original image, and then we use Otsu histogram-based thresholding (see the green contour in Fig. 1(f)).

2.2. Tracking Surfing Virus Particles

To track surfing virus particles, we combine a probabilistic tracking approach based on independent particle filters (IPF) [5] with a discrimination scheme based on the segmentation result of cell filopodia. The intensity distribution of a particle is modeled by a 2D Gaussian function with standard deviation σ_{XY} (radius of a particle). Each tracked particle at time point t is represented by a state vector $\boldsymbol{x}_t = (x_{p,t}, y_{p,t}, I_{max,t}, \sigma_{XY,t})$ which includes the position $\boldsymbol{x}_{p,t} = (x_{p,t}, y_{p,t})$, the peak intensity $I_{max,t}$, and the radius $\sigma_{XY,t}$. Let $(\mathbb{R}^2, d(\cdot))$ be a metric space, where $d(\cdot)$ is the Euclidean distance. Given the binary segmentation result for filopodia S_t at time point t (Section 2.1), we consider a particle at position $\boldsymbol{x}_{p,t}$ to move along cell filopodia if there exists an image point $\boldsymbol{z} \in \mathbb{R}^2$ such that

$$d(\boldsymbol{x}_{p,t}, \boldsymbol{z}) \leq \sigma_{XY,t} \quad \text{and} \quad \boldsymbol{z} \in S_t \quad (4)$$

SNR	CT (%)	MT (%)	ML (%)	TF (%)	FP (%)	OD (%)
8	98	2	0	1	0	1
4	85	14	1	8	6	7

Table 1. Quantitative results of our approach for synthetic image sequences using different performance measures.

Otherwise, the trajectory of the virus particle is terminated at time point $t-1$.

To determine the motion direction of surfing virus particles relative to a cell, we use the fast marching algorithm, where the potential function is $\mathcal{P}=1$ at points which belong to segmented filopodia and $\mathcal{P}=\infty$ elsewhere. As initial contour for propagation, the contour of the segmented cell body is used. The signed value of the displacement of a surfing virus particle is computed as follows:

$$\mathcal{U}(\boldsymbol{x}_t) = \mathcal{U}_1(t, \boldsymbol{x}_t) - \mathcal{U}_1(t-1, \boldsymbol{x}_{t-1}) \tag{5}$$

where $\mathcal{U}_1(t, \boldsymbol{x}_t)$ is the minimal action path between the cell body and the position of the particle at time point t. The sign of $\mathcal{U}(\boldsymbol{x}_t)$ represents the direction of the motion of a virus particle moving towards or away from the cell body. The relative speed of the particle is computed as $v = \frac{\mathcal{U}}{T}$, where T is the time interval between subsequent frames.

3. EXPERIMENTAL RESULTS

Our approach has been applied to synthetic as well as real microscopy image sequences. To quantitatively evaluate the performance, the following measures were calculated: the number of correct trajectories (CT) (i.e., trajectories which start when particles attach to filopodia and finish when they invade cells, and which have no gaps), mostly correct trajectories (MT) (i.e., trajectories which start later than the time point of attachment to filopodia and/or finish before the time point of invasion, which have no gaps, and contain more than 50% of correctly tracked time steps), and mostly lost trajectories (ML) (i.e., trajectories as for MT, but which contain less than or equal to 50% of correctly tracked time steps), as well as the number of trajectory fragments (TF), and the number of false positives (FP) (trajectories of virus particles which do not move along cell filopodia). To quantify cases when tracking of a virus particle is started but the particle has not yet reached filopodia or tracking is not stopped after a virus particle has already reached the cell body, we compute the number of overdetections (OD).

3.1. Evaluation based on synthetic image sequences

The generated synthetic image sequences consist of two channels. The first channel represents a cell which was modeled by a circular shape and straight filopodia with Gaussian intensity cross-sections. The second channel displays moving virus particles. 15 out of 100 particles are moving along filopodia.

ID	CT (%)	MT (%)	ML (%)	TF (%)	FP (%)	OD (%)	N_S
1	92	8	0	8	0	4	13
2	100	0	0	0	0	0	3
3	91	6	3	9	3	5	32
4	94	6	0	11	0	2	18
5	93	5	2	4	3	3	439
6	88	12	0	6	12	6	17

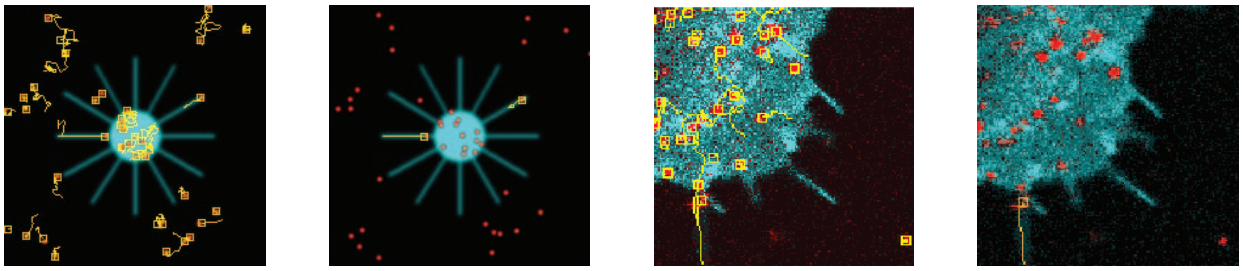
Table 2. Quantitative results of our approach for 6 real microscopy image sequences. N_S denotes the total number of surfing virus particles in an image sequence.

Tracking was performed for two levels of the signal-to-noise ratio (SNR). The computed performance values are shown in Table 1. In the case of a high SNR=8, 98% of the particles were tracked correctly. False positive (FP) detections did not occur due to the good image quality. Also, track fragments (TF) and overdetections (OD) occurred rarely. The performance decreased in the case of the lower SNR=4, however, we still obtain a good result.

We also applied a general tracking approach based on IPF [5] to the same image sequences. Figures 3 (a), (b) show that the results of this approach are not well suited for analyzing the process of virus surfing, since all particles were tracked, in contrast to our approach.

3.2. Evaluation based on real image sequences

We have also evaluated the performance of our tracking approach based on 6 real microscopy image sequences. The images have been acquired using a confocal microscope and consist of 27 up to 401 frames with a time interval between subsequent frames of 15 seconds. These images show ALV-env pseudotyped MLV particles (labeled with YFP) penetrating target cells (XC-cells or 293T-cells stained with CFP). The number of surfing virus particles N_S for an image sequence is in the range of 3 to 439. Ground truth was determined manually. For the image sequences 4 and 5 we used the matched filter for enhancement of thin structures and for the other image sequences we used the vesselness filter (Section 2.1). The quantitative results for the performance are summarized in Table 2. It can be seen that our approach yields a high number of correct trajectories (CT) and a relatively low number of false positive detections (FP) and overdetections (OD) except for sequence 6. Errors are caused by photobleaching effects and inhomogeneity in the intensity structure of filopodia. The mean number of correct trajectories averaged over all 6 image sequences is $\overline{CT} = 93\%$. As a comparison, we also applied a general tracking approach [5] which yielded $\overline{CT} = 0\%$ since tracking is not terminated when virus particles invade a cell. For our approach, we have also computed the speed of motion of surfing virus particles relative to a cell body and have compared the results with manual analysis. Figure 4 shows the result for all 6 analyzed real image



(a) (b) (c) (d)

Fig. 3. Tracking results for (a),(b) a synthetic image sequence and (c),(d) a real microscopy image sequence. (a),(c) Results of a general tracking approach. (b),(d) Results of our approach for tracking surfing virus particles. Cells are represented in turquoise and virus particles are represented in red. Trajectories of particles are shown in yellow.

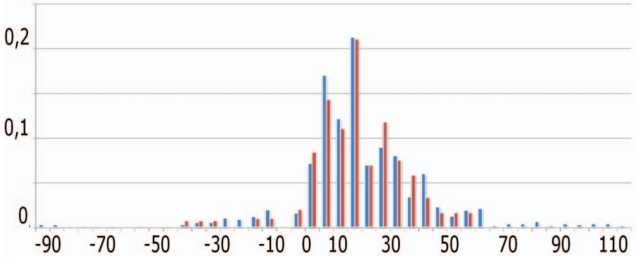


Fig. 4. Normalized histograms of the speed of surfing virus particles relative to a cell body (nm/s) by manual (blue) and automatic (red) tracking for all 6 real microscopy image sequences.

sequences. It can be seen that the two histograms agree well. Thus, the automatic approach produces reliable statistical results. From the histograms we also computed the mean values and standard deviations of the speed. While for manual tracking we obtained $\overline{v}_{man} = 25,8$ nm/s and $\sigma_{v_{man}} = 17,4$ nm/s, automatic tracking yielded $\overline{v} = 22,4$ nm/s and $\sigma_v = 15,6$ nm/s, which is reasonably good result given the challenging image data and task. As an example, in Figure 3, we show the result of our approach for one of the image sequences (Fig. 3(d)) in comparison to the result using a general tracking approach [5] (Fig. 3(c)). It can be seen that our approach tracks only virus particles along filopodia. Experiments were performed on a standard computer with 2.33 GHz CPU and 2 GB RAM. The computation time for an image sequence of 100 frames with a frame size of 512×512 pixels is about 4 minutes which can be further reduced by parallel computing.

4. CONCLUSIONS

We have proposed a novel automatic approach for tracking single surfing virus particles. The approach combines probabilistic tracking of virus particles with segmentation of cell filopodia and exploits information about the positions of virus particles relative to the cell body. The approach was successfully applied to synthetic and live cell microscopy image sequences.

Acknowledgments Support of the BMBF (FORSYS) project VIROQUANT is gratefully acknowledged. We also thank the graduate schools HBIGS and HGS Mathcomp.

5. REFERENCES

[1] M.J. Lehmann, N.M. Sherer, C.B. Marks, M. Pypaert, and W. Mothes, "Actin- and myosin-driven movement of viruses along filopodia precedes their entry into cells," *Journal of Cell Biology*, vol. 170, no. 2, pp. 317–325, 2005.

[2] C.J. Burckhardt and U.F. Greber, "Virus movements on the plasma membrane support infection and transmission between cells," *PLoS Pathog*, vol. 5, no. 11, e1000621, 2009.

[3] I.F. Sbalzarini and P. Koumoutsakos, "Feature point tracking and trajectory analysis for video imaging in cell biology," *Journal of Structural Biology*, vol. 151, no. 2, pp. 182–195, 2005.

[4] N. Arhel, A. Genovesio, K.A. Kim, S. Miko, E. Perret, J.-C. Olivo-Marin, S. Shorte, and P. Charneau, "Quantitative four-dimensional tracking of cytoplasmic and nuclear HIV-1 complexes," *Nature Methods*, vol. 3, pp. 817–824, 2006.

[5] W.J. Godinez, M. Lampe, S. Wörz, B. Müller, R. Eils, and K. Rohr, "Deterministic and probabilistic approaches for tracking virus particles in time-lapse fluorescence microscopy image sequences," *Medical Image Analysis*, vol. 13, no. 2, pp. 325–342, 2009.

[6] E. Rothenberg, L.A. Sepùlveda, S.O. Skinner, L. Zeng, P.R. Selvin, and I. Golding, "Single-virus tracking reveals a spatial receptor-dependent search mechanism," *Biophysical Journal*, vol. 100, no. 12, pp. 2875 – 2882, 2011.

[7] I. Smal, K. Draegestein, N. Galjart, W. Niessen, and E. Meijering, "Particle filtering for multiple object tracking in dynamic fluorescence microscopy images: Application to microtubule growth analysis," *IEEE Trans. on Medical Imaging*, vol. 27, no. 6, pp. 789 –804, 2008.

[8] A. Doucet, N. De Freitas, and N. Gordon, Eds., *Sequential Monte Carlo Methods in Practice*, Springer-Verlag, 2001.

[9] R.F. Frangi, W.J. Niessen, K.L. Vincken, and M.A. Viergever, "Multiscale vessel enhancement filtering," in *Proc. MICCAI'98*. 1998, vol. 1496 of *LNCS*, pp. 130–137, Springer-Verlag.

[10] S. Chaudhuri, S. Chatterjee, N. Katz, M. Nelson, and M. Goldbaum, "Detection of blood vessels in retinal images using two-dimentional matched filters," *IEEE Trans. on Medical Imaging*, vol. 8, no. 3, pp. 263–269, 1989.

[11] L. D. Cohen and R. Kimmel, "Global Minimum for Active Contour Models: A Minimal Path Approach," *Internat. J. of Computer Vision*, vol. 24, no. 1, pp. 57–78, 1997.